Localized Blade-Root IBC for Rotor-Performance Enhancement and Vibration Reduction

Philip Küfmann, Rainer Bartels, Berend G. van der Wall

German Aerospace Center (DLR), Institute of Flight Systems
Lilienthalplatz 7, 38108 Braunschweig
Germany

philip.kuefmann@dlr.de, rainer.bartels@dlr.de, berend.vanderwall@dlr.de

This paper focuses on numerical investigations of the effects of non-harmonic Individual Blade Control (IBC) or Localized Pitch Control (LPC). Different non-harmonic control schemes for the blade-root pitch are presented, optimized for performance enhancement as well as simultaneous vibration reduction and compared to a conventional approach using 2/rev Higher Harmonic Control (HHC). The calculations were performed using the DLR's comprehensive rotor code S4, simulating two different isolated model rotors at an advance ratio of µ=0.32 with a modified Beddoes inflow model and including rotor-fuselage interaction. In simulations with Bo-105 model rotor blades, LPC was found to perform superior to conventional 2/rev HHC, with reductions in required power of up to -3.62% (-2.26% in power and -57.3% in vibration levels during multi-objective optimization). However, when applied to a more modern rotor blade the margins for power savings as well as vibration reduction were found to be significantly lower.

NOTATION

BVI	Blade Vortex Interaction
DLR	Deutsches Zentrum für Luft- und Raumfahrt (German Aerospace Center)
DNW	Deutsch-Niederländischer Windkanal (German Dutch Wind Tunnel)
FTK	Fortschrittliche Taumelscheiben-Konzepte (Advanced Swashplate Concepts)
HHC	Higher Harmonic Control
IBC	Individual Blade Control
LLF	Large Low-Speed Facility
META	Mehrfach-Taumelscheibe (multipleswashplate control system)
TEF	Trailing Edge Flaps

SYMBOLS

A_{dip}	Dip amplitude
$A_{HHC,2}$	2/rev HHC amplitude
$F_{X,Y,Z}$	Rotor hub forces
L/D_{eff}	Effective lift-to-drag ratio
$M_{X,Y,Z}$	Rotor hub moments
α_{eff}	Effective angle of attack
Φ_{dip}	Dip phase angle
$\Phi_{1,2,H}$	Widths of dip sections
$\varphi_{HHC,2}$	2/rev HHC phase
ψ	Rotor azimuth
$\Psi_{1,2,a,b}$	Azimuthal positions
ϑ_i	Angle of incidence of blade i
$\Theta_{0,C,S}$	Primary Control Coefficients

1. INTRODUCTION

While in many ways more versatile than most fixed wing aircraft and having unique properties such as the capability to hover – helicopters are also affected by a very specific set of problems including high vibration levels, noise emissions and high power consumption.

These problems can be attributed to the highly asymmetric flow field encountered by the rotor blades during forward flight, leading to a non-uniform, asymmetric distribution of lift and drag over the rotor disk. The resulting aerodynamic phenomena such as blade-vortex interaction stall and dynamic stall effects on the retreating side of the disk and high Mach-numbers on the advancing side are the main cause for the problems mentioned above.

Measures to reduce the high power consumption of helicopters are either of passive or active nature. Passive measures mainly consider the design of aerodynamically more advanced and efficient nacelles, fuselages [1], rotor hubs (which alone often accounts a major percentage of the overall parasitic drag [2]) and fairings for external components as well as optimized rotor blade designs.

Active measures are aimed at modifying the rotor blades' movement and angle of attack by applying additional, high-frequency control inputs during flight. Work considering the use of active rotor

control for rotor performance enhancement goes back to the 1950s [3] and 60s [4] and was mostly focused on the application of HHC-signals which solely comprise of a linear combination of the integer multiples of the rotor frequency (n/rev).

Numerous successful studies have been performed aimed at performance enhancement by HHC and later IBC, including numerical investigations, [5]–[7] experimental investigations [8] as well as wind tunnel experiments [9]–[14] and flight tests [15]–[20]. Concerned mainly with harmonic control functions, those studies found the second rotor harmonic, 2/rev, the most advantageous control function for power reductions.

For example, full-scale Wind tunnel tests carried out by Eurocopter Deutschland (ECD) and with a modified, IBC-capable Bo-105 rotor [12], [13] yielded power reductions of 7% at an advance ratio of µ=0.4 with a 2/rev amplitude of 1°. Later, flight tests with an IBC-capable CH-53 helicopter performed by ZFL and the WTD61 of the German Bundeswehr yielded a power reduction of approximately 6% with a 2/rev amplitude of only 0.67°. [18]–[20].

In most studies, the reduction of profile drag at the advancing side of the rotor disk and the redistribution of instationary airloads were identified as the main contributors to the performance enhancements achieved with 2/rev HHC, while stall reduction on the retreating side played only a minor role.

However, the 2/rev HHC control inputs not always had exclusively positive influence on the rotors aerodynamics. It was found that in spite of the overall performance enhancement achieved, 2/rev HHC could be responsible for increased profile drag in certain azimuthal sections [6], [12] and also in some cases promoted the onset of stall on the retreating side of the rotor disk [6], [8], [21]. These side effects suggest that 2/rev HHC might not be the optimal control function for rotor performance enhancement and that a more tailored function, which addresses the problems more locally might be of advantage.

A study performed by Yeo [22] concerning the potential of different active control methods for power reductions showed that discrete, non-harmonic control schemes can be highly beneficial when used in combination with active gurney flaps.

Work by Malovrh and Gandhi [23] also shows the great potential of non-harmonic discrete active control for BVI-noise reduction. Recent work by Kody et al. [24] covers the numerical optimization of a non-harmonic control function for single and double trailing edge flaps, yielding power reductions of approximately 10% using a uniform inflow model. Besides power reductions, vibrations were also taken into account, and simultaneous reductions in power and vibrations levels were achieved.

In contrast to work regarding the non-harmonic control of trailing edge flaps (TEF), microflaps or gurney flaps, this paper is concerned with non-harmonic control inputs introduced at the blade root by a classic HHC/IBC system.

Different forms of non-harmonic, Localized Pitch Control (LPC) are presented and evaluated numerically regarding their potential for reducing rotor power during medium to high-speed forward flight. The aerodynamic effects leading to the power reductions are analyzed and discussed, as well as the effects of LPC on vibration levels at the rotor hub in the non-rotating frame (fuselage).

Two different model rotor blades were used in the study (see 2.2), allowing for an examination of the influence of rotor blade design on the potential for power reductions by LPC. Additionally, the results of optimizations of the different LPC control functions and conventional 2/rev HHC performed with the objective to either reduce rotor power or rotor power and vibrations simultaneously are presented in this paper.

2. NUMERICAL TOOLS

2.1. The DLR's Rotor Simulation Code S4

DLR's high resolution 4th generation rotor simulation code (S4) has its origins in the mid-'70s with rigid flapping, constant downwash, and steady table look-up of aerodynamic coefficients. Today, S4 is used for analysis of any kind of active rotor control with respect to performance, dynamics, and noise [25] and for support of wind tunnel testing.

2.1.1. Structural Mechanics

The structural dynamics modeling consists of two parts. First, a finite element method (FEM) [26] based on the Houbold-Brooks formulation [27] acts as off-line pre-processor and performs the modal analysis, i.e., it computes the coupled mode shapes and natural frequencies *in vacuo*. In a second step,

the rotor simulation itself solves the dynamic response problem of these modes (which are reduced to their major component) subjected to the aerodynamic loading in the form of a modal synthesis.

2.1.2. Section Aerodynamics

For two-dimensional unsteady compressible section airloads, a semi-empirical analytic formulation of the airfoil coefficients C_nM^2, C_mM^2, and C_tM^2 is used within S4. The respective unsteady transfer functions of step inputs are applied (Wagner function for the airfoil motion [28] and Küssner function for the gust [29], both with compressibility corrections), and the effective angle of attack is computed using the Duhamel integral formulation [30]. Validations of the model for dynamic stall were performed in [31]–[33].

The tip loss of lift is accounted for in the outer 5% of the blade by modifying the induced velocities progressively towards the tip such that the zero lift angle of attack is obtained there. Also, fuselage interference flow is computed at the blade sections by an analytical formulation derived from potential theory calculations [34]. Within this study, the HART II fuselage was taken into account which recently was modeled and included in S4 [35], based on Navier-Stokes data.

2.1.3. Rotor Wake

To address the modifications of induced velocities due to active rotor control (like HHC and LPC) a modified form of Beddoes' prescribed wake geometry formulation [36] was utilized instead of the simpler Mangler/Squire model [37]..

Furthermore, the interference of the HART II fuselage with the wake geometry is taken into account [38] and was also used for all calculations using the Beddoes wake model presented in this paper.

2.1.4. Trim Computation

The rotor trim is performed to match the experimental hub forces (F_z, F_x and F_y in wind tunnel coordinates) by means of time integration based on a 4th-order Runge-Kutta scheme with azimuthal increments of 2° (intermediate step at every 1°). The wake geometry is updated once a trim cycle with associated blade motion and airloads is finished and the influence coefficients of the new wake geometry are updated before the next trim cycle starts. During

the trim, the induced velocities of the far wake are updated every few revolutions to account for the variations of changing airloads and modified vortex strengths.

2.2. Blade Models

In the framework of the nationally funded research project FTK ("Fortschrittliche Taumelscheiben-Konzepte, Advanced Swashplate Concepts) in cooperation with airbus helicopters, rotor tests will be conducted at the DLR's own test facility as well as in the Large Low-Speed Facility (LLF) wind tunnel of the DNW.

During those tests a proven set of rectangular model rotor blades as well as a set of new model rotor blades with modern geometry and profiles will be used for the purpose of comparison. Due to this, the S4 calculations presented here also were performed for these two different sets of rotor blades.

The first set of Mach-scaled rotor blades is geometrically and dynamically realized as close as possible to the original rectangular Bo-105 rotor blades with a scale of 1:2.45. Due to Reynolds number effects, the blade chord is 10% larger than geometrically scaled. The basic rotor blade data is given in Table 1.

Table 1: Basic data of the Mach-scaled Bo-105 model rotor blades used in HART II campaign [39]

|	
Rotor radius R	2m
Blade chord c	0.121m
Twist θ_{TW} (outboard r/R=0.22)	-6.24° (linear)
Airfoil	NACA23012
Rotor system	hingeless
Rotational speed Ω_{ref}	109 rad/sec
flapping mode frequency [*] 1st 2nd 3rd 4th 5th	1.125 2.839 5.171 8.050 11.520
lead-lag mode frequency [*] 1st 2nd 3rd	0.782 4.592 11.584
torsion mode frequency [*] 1st 2nd	3.818 10.097

[*] normalized to 100% rotational speed, coupled calculation

The second and new set of modern model rotor blades draws on the blade geometry and profiles of the EC145-C2 and the ATR rotor [40]. According to the project name this blade is called FTK-blade. Compared to the rectangular model blades of the Bo-105 the planform of the FTK-blade has inboard tapering and features a back-swept parabolic tip (see Figure 2-1). Due to the planned wind tunnel tests on the same rotor test bed the scale of the FTK-blades is 1:2.75, with a 5% larger blade chord than geometrical scaled. In Table 2 the main data of the FTK-blades are summarized.

Table 2: Basic data of the Mach-scaled FTK-blades

Rotor radius R	2m
Equivalent blade chord c_{equiv}	0.124m
Twist	-12°/R
Airfoil	OA series
Rotor system	hingeless
Rotational speed Ω_{ref}	110.4 rad/sec

Figure 2-1 shows the planforms of both used model rotor blades in comparison.
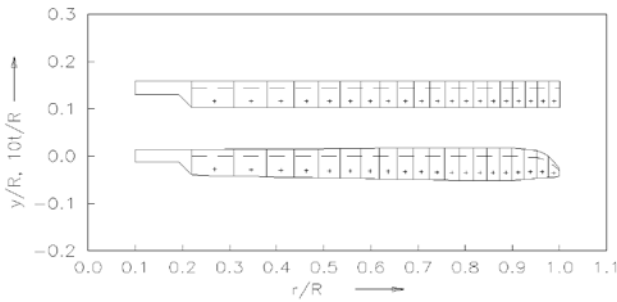
Figure 2-1: Planforms of Bo-105 (top) and FTK (bottom) model rotor blades

Even though the FTK model blade is derived from an EC145-C2 rotor blade (which has a different reference rotational speed than the Bo-105 rotor blade), all calculations were done using the rotational speed of the Bo-105 model rotor in order to keep the tip speed constant and thus make the results for the different model blades more comparable.

In the computations shown in this paper, five flap modes, three lag modes, and two torsion modes have been retained for the Bo-105 model blade, and five flap modes, three lag modes and the first torsion mode for the alternative FTK model blade. Since the FTK model blade exhibits a much higher overall torsional stiffness than the Bo-105 model blade, a higher torsional mode was not considered, since its deflection was too small to contribute to the results.

Unless otherwise noted, the results presented were obtained using the Bo-105 model blade, the results obtained with the FTK model blade are summarized in 4.4 separately.
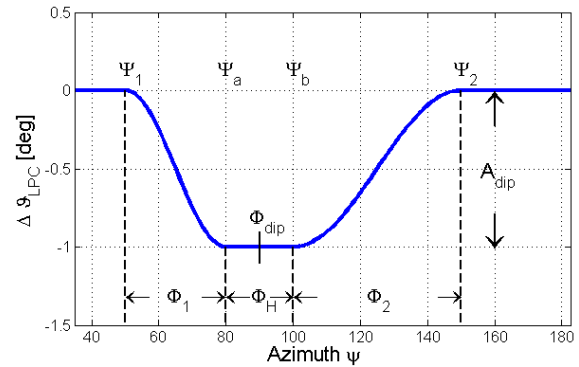
3. FORMULATION OF LPC FUNCTIONS

Two different LPC control schemes were formulated for the study, which manipulate the blade pitch in one and two sections of the rotor disk, respectively.

3.1. Single dip

The basic form of those so called "dips" is dependent on four parameters indicating the magnitude A_{dip} and azimutal position Φ_{dip} of the localized pitch variation, the width of the cosine-slopes leading into and out of the affected sector (Φ_1 and Φ_2) and the azimuthal width Φ_H of an optional plateau in the course of the LPC-function.

To avoid discontinuities in the LPC-function, the widths of the slopes (Φ_1 and Φ_2) were set to a minimum value of 5°.

Figure 3-1: Basic form of LPC control function

For the calculation of the control function, which is superimposed on the primary controls for each rotor blade, those parameters are converted into four azimuthal positions, $\Psi_{1,2,a,b}$, see Figure 3-1.

For each blade i, the pitch variation due to LPC is computed as follows:

(1)
$$\Delta\vartheta_i = -\frac{1}{2}A_{dip}\left(1 - \cos\left(\frac{2\pi\psi_i}{2\Phi_1}\right)\right)$$
$$for\ \Psi_1 < \psi_i \leq \Psi_a$$

(2)
$$\Delta\vartheta_i = -A_{dip}$$
$$for\ \Psi_a < \psi_i \leq \Psi_b$$

$$(3) \quad \Delta\vartheta_i = \frac{1}{2}A_{dip}\left(1 - \cos\left(\frac{2\pi(\psi_i - \Psi_b)}{2\Phi_2}\right)\right)$$

$$for \ \Psi_b < \psi_i \leq \Psi_2$$

3.2. Two separate dips

The second LPC-function consists of two independent dips (formulated as described above), which can be separately configured and positioned around the rotor azimuth.

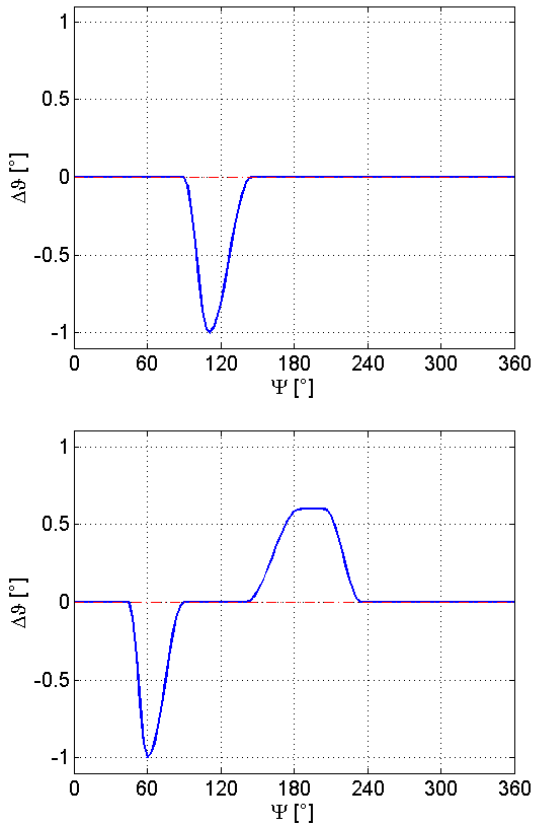Figure 3-2 shows examples of each LPC-function used for the calculations presented in this paper.

Figure 3-2: Examples of the two different LPC-functions

4. NUMERICAL INVESTIGATIONS

4.1. Simulation setup

Since the DLR's rotor code S4 was used to simulate an isolated model rotor (instead of a complete helicopter) under wind tunnel conditions the necessary trim conditions (forces and moments at the rotor hub) had to be identified beforehand.

This was achieved by the evaluation of simulation results obtained from the "Helicopter Overall Simulation Tool" (HOST) [41]. For the baseline case,

a full-scale Bo-105 helicopter was simulated in level flight with a flight speed of 250km/h (μ = 0.32), a mass of 2.5to and a C_T/σ of 0.0771.

The forces and moments at fuselage resulting from the trim procedure in HOST were then Mach-scaled in order to obtain the correct values for the simulation using a scaled wind tunnel model of the Bo-105 rotor system. Those values were subsequently transformed from rotor coordinates to wind tunnel coordinates using the Euler's-angles of the fuselage from the HOST-simulation and the Bo-105's shaft angle of -3°.

In order to keep the lift and the propulsive force constant during the calculations, the resulting hub forces F_X, F_z and F_y were chosen as trim conditions for all calculations.

4.2. Parameter variation study

For the first set of calculations the parameters of the different LPC functions were varied systematically over a predetermined range for both inflow models:

Table 3: Range of LPC parameters for parameter variation study

LPC variant 1 (single dip)			
Parameter	Min.	Max.	Step
A_{dip}	-1°	1°	N/A
Φ_{dip}	0°	345°	15°
Φ_1	10°	55°	15°
Φ_2	10°	55°	15°
Φ_h	0°	15°	30°
LPC variant 2 (two separate dips)			
A_{dip}	-1°	1°	N/A
Φ_{dip}	0°	345°	15°
Φ_1	10°	55°	15°
Φ_2	10°	55°	15°
Φ_h	0°	15°	30°

Since the first calculations using the Mangler/Squire inflow model yielded unrealistically high power savings for LPC as well as for 2/rev HHC (>10% at 1° amplitude) it was decided to rely entirely on the computationally more expensive but also much more sophisticated Beddoes inflow model (see 2.1.3) for further calculations.

In order to keep the computational effort to a reasonable level while covering a wide range of possible azimuthal positions and dip contours (due to different slope angles), the amplitude settings

were limited to for 1° positive and negative pitch variation, respectively.

While not yet utilizing the full potential of the LPC-functions for performance enhancement and vibration reduction, these initial calculations yielded the first reference points for advantageous azimuthal positions and forms of the two LPC-functions. Furthermore, the 'best-case' parameter sets for each case were later used as the initial parameter sets for single- and multi-objective optimization (see 4.3).

For comparison to 2/rev HHC, additional calculations were performed with an amplitude $A_{HHC,2}$ of up to 1° and a phase $\varphi_{HHC,2}$ ranging from 0° to 345° in 15° steps.

4.2.1. Basic effects of LPC on rotor performance and vibration levels

The baseline case for the 250km/h case with Bo-105 type rotor blades shows a clear area of heightened sectional torque contribution $C_d r M^2$ at approximately 60 degrees azimuth (see Figure 4-1 and Figure 3-1), as a result of high profile drag within the blade tip area.
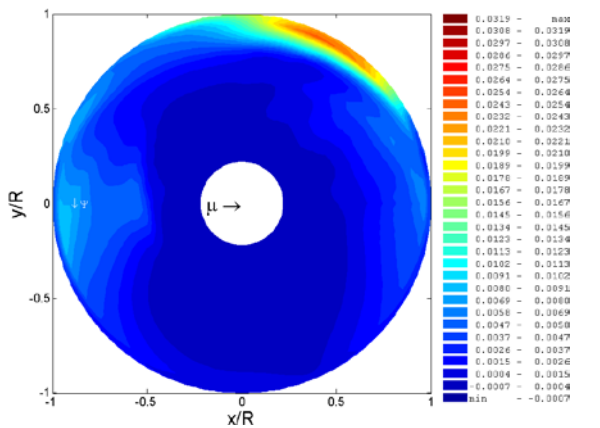

Figure 4-1: Sectional torque contribution CdrM² for the baseline Bo-105 case

A second, although much less pronounced area of heightened profile drag can be found around 190 degrees azimuth. The baseline rotor power P for this case was 93.82kW.

The best LPC solution for the reduction of required rotor power found via parameter variation were two separate dips, lowering the blade pitch between 15 and 45° azimuth and increasing pitch at 315° azimuth, as depicted below, resulting in a reduction of rotor power of 3.25kW or 3.46% compared to the baseline case. The best cases for the single dip

solution and 2/rev HHC yielded power reductions of 2.88% and 3.50%, respectively.
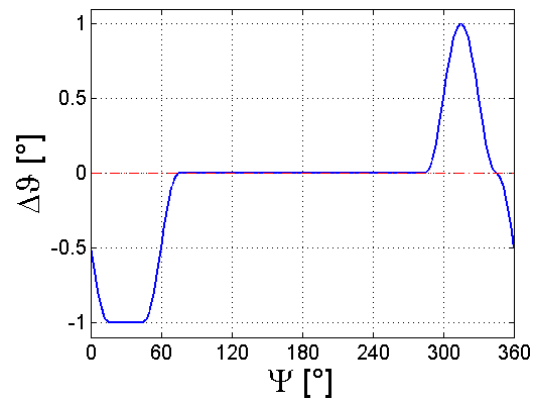

Figure 4-2: Best LPC function for power reduction found during parameter variation

The resulting distribution of the sectional torque contribution over the rotor disk clearly shows reductions at the 60° and 180° azimuth locations resulting from a change in the angle of attack (and thus a change of C_d) within those regions.
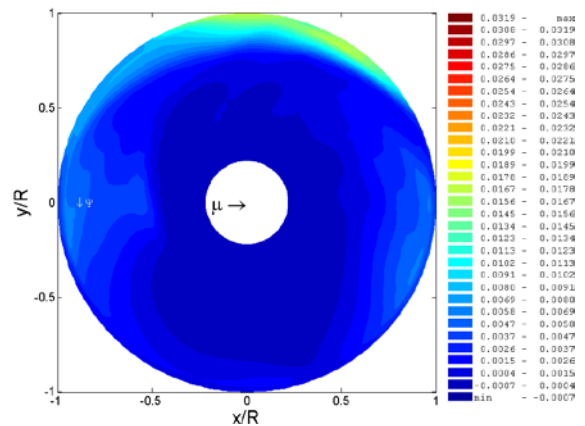

Figure 4-3: Sectional torque contribution for optimum LPC (two separate dips)

While the change in the angle of attack at 60° degrees is a result of the LPC function itself, the change at the 180° position can be attributed to the change in 1/rev primary control in order to maintain rotor trim and the introduction of a 2/rev component by the form of the applied LPC function. This can be seen from the plot of the change of the effective angle of attack at 96% radius, see Figure 4-4:
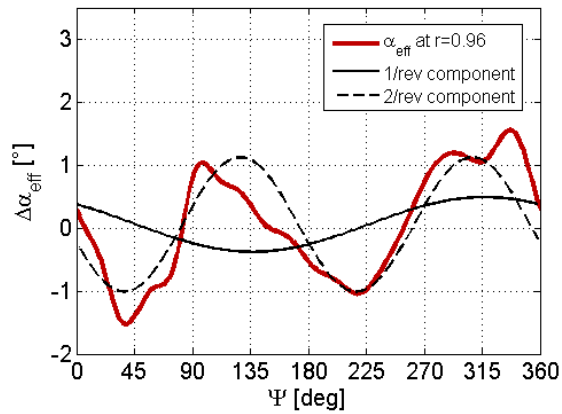
Figure 4-4: Change in angle of attack at 96% radius

The application of the best LPC function found for power reduction also resulted in an overall reduction of vibration levels, taking into account the first, second and third rotor harmonics (4/rev, 8/rev and 12/rev) of all six rotor hub forces and moments, see Figure 4-5.
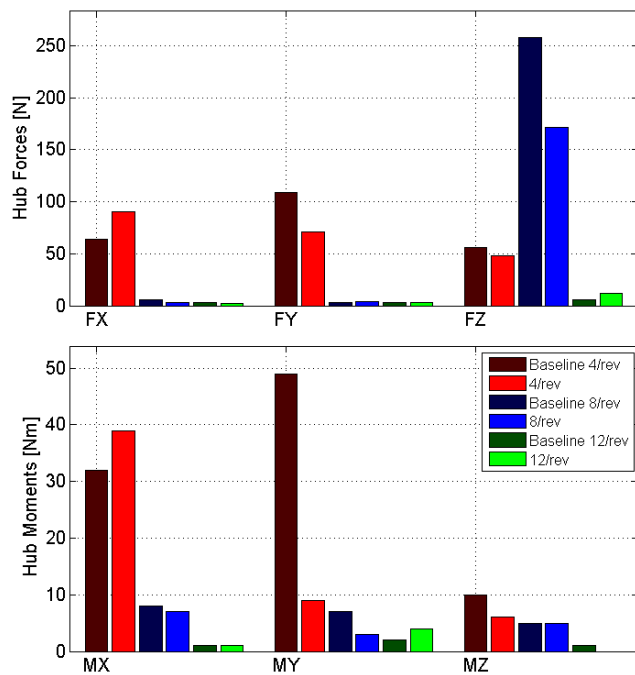
Figure 4-5: Changes in vibratory loads due to LPC

On closer inspection however those reductions mainly affected the 8/rev content of the vertical force F_Z as well as the first harmonics of F_Y and M_Y, whereas the first harmonics of both F_X and M_X were increased.

This shows that in an evaluation of the potential of LPC function for rotor performance enhancement the resulting changes vibratory loads cannot be neglected and thus have to be considered for the optimization procedures described in 4.3.

4.2.2. Effects of LPC on rotor trim conditions

Using the data obtained from the parameter variation study, the influence of LPC on the rotor trim was examined.

For every calculated HHC and LPC case the resulting primary control inputs Θ_0, Θ_C and Θ_S from the S4 trim procedure were compared to the trim solution for the respective baseline case.

As an example, the trim deviations resulting from a single dip with a width of 60 degrees (30 degrees for each slope) and an amplitude of 1° are examined in this paper.

In this case, the deviations in rotor trim did not exceed 0.3° for the collective and 0.6° for the lateral trim, and turned out to be slightly less than the trim deviations for 2/rev HHC with the same amplitude (max. 0.32° for collective and 0.68° for cyclic trim).
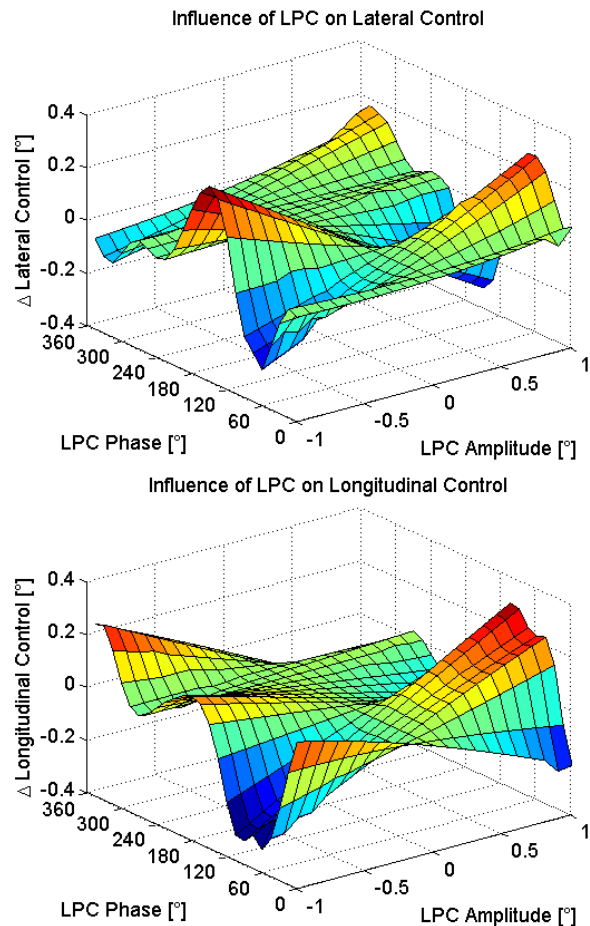
Figure 4-6: Influence of LPC single dip function on cyclic trim

While the influence of the single dip LPC function on collective control shows a fairly linear correlation with the applied amplitude for all phase angles (or

azimuthal positions of the dip), the deviations in longitudinal and lateral control show clear maxima/minima at a phase angle of 60° and 190° (see Figure 4-6). This corresponds fairly well to the previously found locations of maximum sectional torque contribution in the baseline case (see Figure 4-1).

This in turn means that if the LPC function is formulated in a way to address those azimuthal locations specifically, the resulting chances in cyclic trim will be at or at least near their respective maximum.

To be able to predict the chances in rotor trim for each LPC function, an effort was made to approximate the resulting changes of the primary control inputs on the basis of the applied LPC parameters.

For the approximation, the functions were converted into their n/rev lateral and longitudinal components (similar to the formulation of a HHC-signal) using the azimuthal position of the dip(s) and the area enclosed by the LPC-curve. The area F_{dip} was used instead of the dip amplitude to be able to account for the width of the pitch variation.

$$C_{dip,n} = F_{dip} \cos(n\Phi_{dip})$$

(4) $$S_{dip,n} = F_{dip} \sin(n\Phi_{dip})$$

$$for\ n = 1 - 4$$

Those components were then used to approximate the resulting changes in the primary control coefficients Θ_0, Θ_C and Θ_S using a polynomial approach:

(5) $$\Delta\Theta_{0,C,S} = \sum_{n=1}^{4} a_n C_{dip,n} + b_n S_{dip,n} + C$$

This approach proved useful for predicting the changes of the primary control coefficients resulting from the application of LPC with an average error of less than 0.05°.

Due to the nature of the trim procedure implemented in the rotor code S4, this approach could not be used to speed up the trim process for LPC calculations, but might prove useful for future applications of LPC, especially in wind tunnel tests, where automatic trim corrections can lessen the workload of the test operator and thus provide additional safety.

4.3. Optimizations

4.3.1. Algorithms used in this study

For the optimization of LPC parameters, both the differential evolution (DE) algorithm by Storn and Price [42] as well as the MATLAB implementation (*fminsearch.m*) of a simplex method [43] were used.

The DE-algorithm is an evolutionary algorithm mimicking the natural evolution process of population members (parameter sets) over several generations.

The initial population consists of a number of parameter sets which carry their respective parameter values as "genes". In case a parameter variation study was performed for the corresponding simulation case (same inflow, speed, rotor, etc.) the previously found "best-case" parameter set regarding the cost-function (see 4.3.3) was used for producing the initial population by random "mutations" of the respective parameters.

The initial population is evaluated by assigning a value for the previously determined cost function to each population member. These values are then used to determine the most promising population members to be carried on to the next generation.

This next generation of parameter sets is generated by two basic mechanisms – the recombination of "genes" (parameters) and random, spontaneous mutation. The former ensures that advantageous genes get carried on while the latter is introduced to ensure the search of the whole parameter space as well as to prevent the optimization algorithm from converging to a local minimum.

Once a minimum has been found by the DE-algorithm, the simplex optimizer takes over, an searches in the vicinity of the previously found "optimal" parameters for further local minima.

4.3.2. Implementation

The optimization algorithm was not directly implemented within the rotor simulation, but was implemented in MATLAB code and coupled with the FORTRAN-based rotor code S4 via in- and output files, as depicted in Figure 4-7.
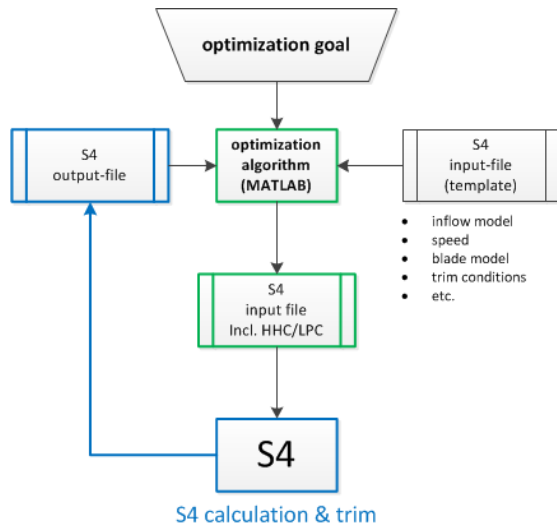
Figure 4-7: Schematic of the coupling between the optimization algorithm and S4

In each computation step, the optimization algorithm modifies the LPC parameters (by choosing the next member of the current population) and updates a template of the S4 input file (which contains all conditions necessary for the trim calculation as well as information about the chosen blade model, inflow model, etc.) with the newly generated parameter set.

Within S4, those parameters are then used to generate the according LPC function superimposed on the primary controls. As soon as the rotor is fully trimmed, S4 creates several output files, which are used to calculate the cost-function previously defined for the optimization. After evaluating the cost function for all members of one population (and dependent on the optimization goal and constraints) a new, updated population of parameter sets is created and the cycle is repeated with the new generation.

After a predetermined number of function evaluations (for both algorithms) the optimization is terminated. To double-check the result, the found optimal parameter set is used for a single S4 calculation outside the optimization cycle and compared to the previously found optimum.

4.3.3. Single objective optimization

The single objective optimization was set to minimize rotor power P [kW] at the rotor shaft for the chosen simulation case using the different LPC-functions, as well as 2/rev HHC.

The limits of the DE-algorithm were set to a maximum of 25 "generations" of parameter sets,

each generation containing 10 members for each parameter of the examined control function.

This lead to a maximum number of function evaluations of 500 for 2/rev HHC (amplitude and phase) as well as 1250 and 2500 for the two LPC variants (5 and 10 parameters, respectively), with each data point taking approximately 30-45 seconds to compute. In each case, another 100 function iterations were performed using the simplex algorithm.

The following table summarizes the constraints of the various HHC and LPC parameters used during the optimization calculations:

Table 4: Parameter constraints for single and multiple-objective optimizations

| Parameter	Min.	Max.
A_{dip}	-5°	5°
Φ_{dip}	0°	345°
Φ_1	10°	55°
Φ_2	10°	55°
Φ_h	0°	15°

The maximum power reduction was achieved using the first LPC variant (single dip) with an amplitude of 1.86° lowering the pitch between 333° and 87° azimuth, as shown in Figure 4-8.
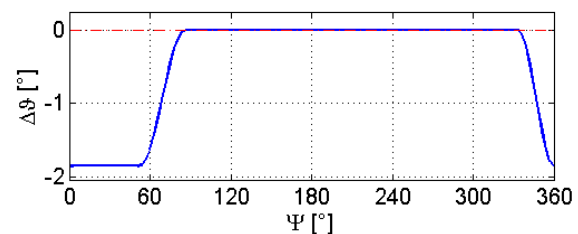
**Figure 4-8: Optimum LPC-function (single dip) for power reduction**

Compared to the baseline (Figure 4-1) the sectional torque contribution was significantly reduced in the first quadrant of the rotor disc and also at the 180° position, while being slightly increased around 105° azimuth (see Figure 4-9)

Similar to the case discussed in 4.2.1 the reduction in the first quadrant can be attributed to the dip itself, while the reduction at the 180° position is a result of the modified primary controls to ensure rotor trim.
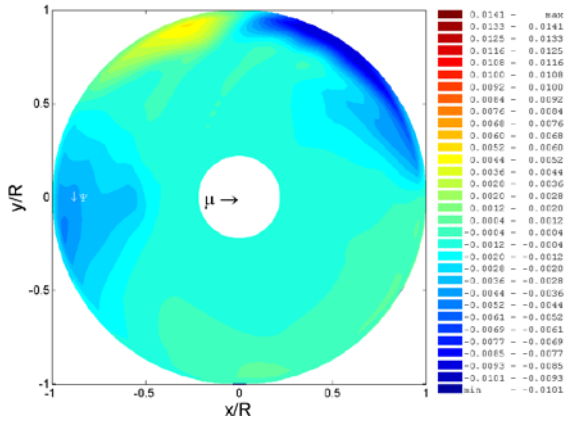
Figure 4-9: Reduction of sectional torque contribution CdrM² compared to the baseline case

Another consequence of the application of the single dip LPC was a redistribution of lift over the rotor disk, as can be seen in Figure 4-10:
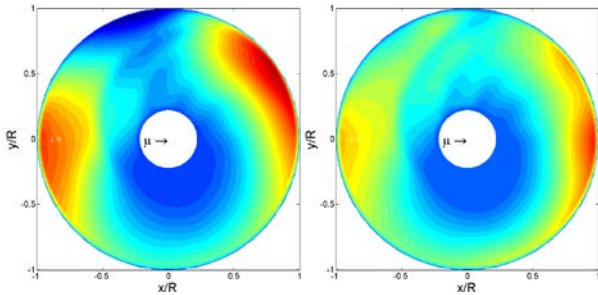

Figure 4-10: Distribution of sectional lift contribution CIM², baseline case (left), single dip LPC (right)

Lift was redistributed from the most heavily loaded sections of the rotor disk mainly to the beginning of the second quadrant, where negative lift was produced in the baseline case, leading to a more uniform distribution over the rotor disk.

As a result, the application of single dip LPC yielded a power reduction of 3.62% and increased the effective lift to drag ratio of the rotor from 5.27 (baseline) to 5.6 (+6.26%), with

$$(6) \qquad L/D_{eff} = \frac{L}{\frac{P_{Rotor}}{V} - F_X}$$

As during the parameter variation studies, the overall vibration levels were reduced (-26%), but with the increase of 4/rev F_X and M_X still present, see Figure 4-11.
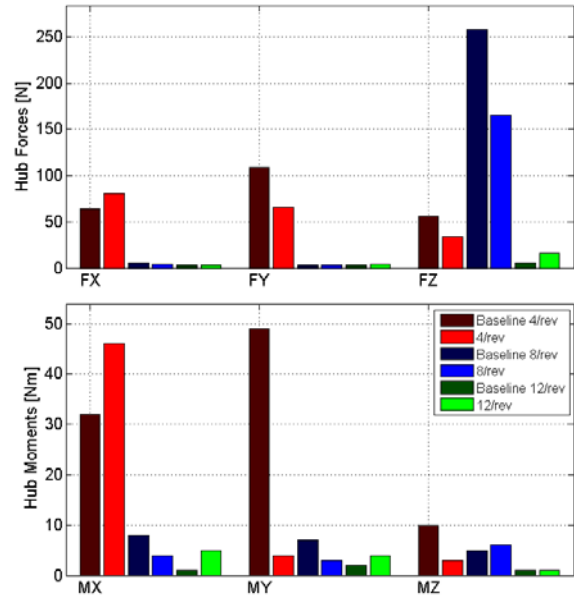
Figure 4-11: Changes in vibratory hub loads due to optimum single dip LPC

The overall results of the single-objective optimizations regarding power reductions are summarized in the following table.

Table 5: results obtained by single objective-optimization

Control Function	ΔP [%]	ΔVibrations 2/4/8/rev [%]	ΔL/D$_{eff}$ [%]
LPC1 (single)	**-3.62**	**-26.0**	**+6.34**
LPC2 (double)	-3.57	-19.4	+6.11
2/rev HHC	-3.50	-23.5	+6.13

It should be noted that although 2/rev HHC performed only slightly inferior to the two LPC variants with regards to reduction of required rotor power, it was the only control function where the 4/rev component of the vertical force F_Z, being the most important vibratory load in 4-bladed helicopters, was slightly increased instead of reduced.

4.3.4. Multiple objective optimizations

For simultaneous reduction of rotor power P and vibration levels the 4/rev, 8/rev and 12/rev amplitudes of all six forces and moments were taken into account and integrated into the cost function:

$$(7) \qquad F_C = P_{Rotor} + \sum_{s=X,Y,Z} A_{Fs,n} + A_{Ms,n}$$

$$for \; n = 4,8,12$$

The limits and constraints for the optimization process and the parameters were the same as for the single objective optimizations.

For the multiple-objective optimization cases, the differences between conventional 2/rev HHC and Localized Pitch Control became even more evident. While the reductions in rotor power achieved with the LPC functions were not as high as in the respective single-objective optimization cases, the power reduction for 2/rev HHC were nearly zero.

**Table 6: results obtained by multiple-objective optimization**

Control Function	ΔP [%]	ΔVibrations 2/4/8/rev [%]	ΔL/D$_{eff}$ [%]
LPC1 (single)	-1.66	-54.8	+0.148
LPC2 (double)	**-2.26**	**-57.3**	**+0.204**
2/rev HHC	-0.02	-51.1	+0.115

In the multiple-objective optimization case, the best results were achieved with the second type of LPC containing two separate dips, shown in Figure 4-12.
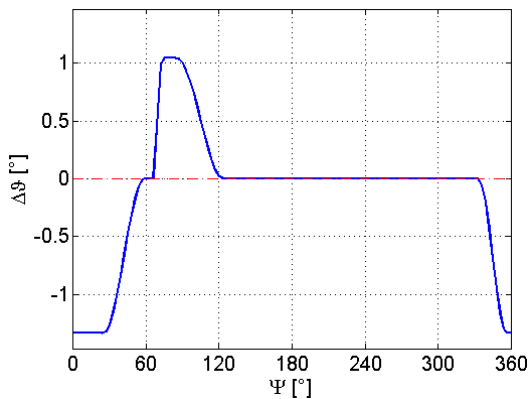

Figure 4-12: Optimum LPC function for simultaneous power and vibration reduction

The mechanisms for the power reduction are the same as described before, local reduction of profile drag (see Figure 4-13) and a redistribution of lift over the rotor disk. While the first dip of the LPC function addresses the high profile drag in around 60° azimuth from the baseline case (Figure 4-1), the second dip significantly increases the angle of attack and thus the profile drag at the beginning of the second quadrant. Furthermore reduction of drag at the 180° position is less prominent than for the single-objective optimization case.
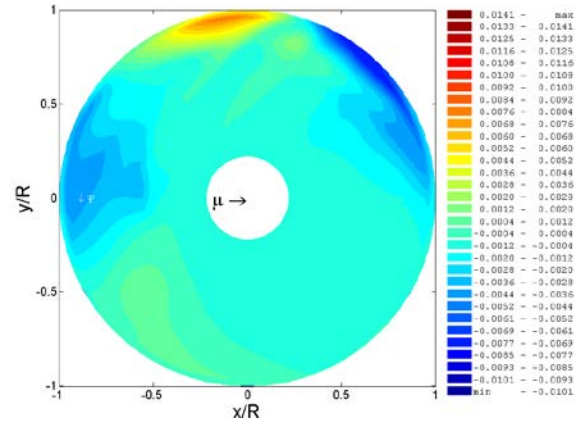
Figure 4-13: Change in CdrM² due to LPC function obtained by multi-objective optimization

Since the sharp increase of the pitch angle at 80 degrees azimuth is not beneficial in terms of power reduction, it must be a result from the second objective of the optimization – the reduction of vibratory loads.
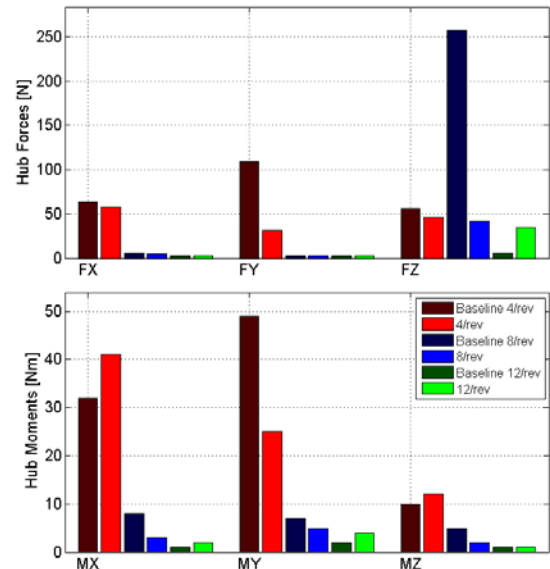
Figure 4-14: changes in vibratory loads due to LPC function obtained by multi-objective optimization

Overall the reduction of vibratory forces and moments was higher than for the single-objective optimization, although a slight increase of the 4/rev components of M_X and M_Z still persisted. The highest increase in vibratory loads was found to be the 12/rev component of the vertical force.

In general the results obtained via multi-objective optimization for power and vibration reduction favor LPC over 2/rev HHC, although not all components of the vibratory loads could be reduced. This issue can presumably be resolved by applying a weighting

function for the different vibration components into the cost function.

4.4. Results obtained with the FTK-blade

For the FTK-blade, the same investigations were conducted as for the Bo-105 blade with both single and multiple-objective optimizations. Due to the more advanced blade design the baseline rotor power P for μ=0.32 already was significantly lower (75.8kW) than for the baseline Bo-105 case (93.82kW) and also exhibited a better effective L/D ratio of 7.71 (Bo-105: 5.27).
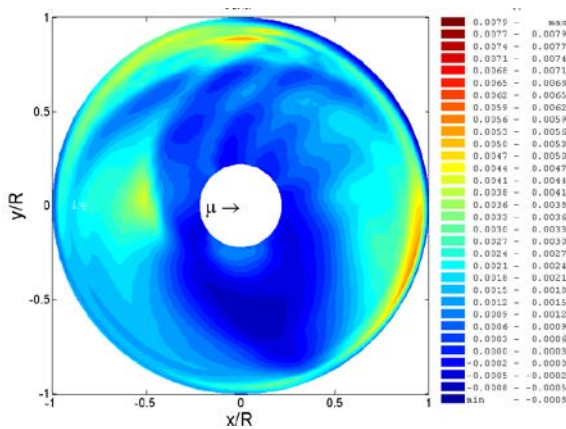

Figure 4-15: Sectional torque contribution CdrM² for the baseline FTK case

Also, the areas of increased sectional torque contribution within the rotor disk were much less pronounced. Correspondingly, the baseline case for the FTK-blade exhibited almost 38% lower vibration levels than the Bo-105 baseline case. As was expected, the margin for additional power and vibration reductions through the application of active rotor control was much lower using the FTK model blade.

The single-objective optimizations for power reduction yielded only very minor power savings of up to 0.52%, combined with (in case of single dip LPC significant) increases in overall vibration levels, and no significant increases in the effective lift-to-drag ratio.

The results obtained from multi-objective optimizations showed that none of the examined control functions was able to simultaneously reduce power and vibration levels. In all "optimum" cases vibrations were reduced, but power consumption was increased by up to 1.66% in case of 2/rev HHC, and the effective L/D ratio was slightly reduced.

For both optimization strategies, the second LPC variant (two separate dips) was found to be the best compromise between moderate reductions of vibrational loads and reduction (or the least increase) in rotor power. The combined results of the optimization efforts are summarized in the following table:

Table 7: Summary of optimization results obtained with the FTK-blade

Control Function	ΔP [%]	ΔVibrations 2/4/8/rev [%]	ΔL/D$_{eff}$ [%]
Single objective optimization			
LPC1 (single)	-0.52	+42.3	+1.01
LPC2 (double)	**-0.41**	**-6.8**	**+0.78**
2/rev HHC	-0.32	+4.4	+0.65
Multiple objective optimization			
LPC1 (single)	+0.55	-26.6	-1.04
LPC2 (double)	**+0.05**	**-22.7**	**-1.30**
2/rev HHC	+1.66	-14.0	-3.11

The main reason for the very low power reductions achieved with the FTK-blade lies in its advanced geometry. Compared to the Bo-105 blade, where the most significant contributions to rotor torque were generated at the rectangular blade tip, the FTK-blade's parabolic swept tip already accounts for drastic reductions in local drag an thus overall rotor torque (see Figure 4-15), leaving less room for improvement.

5. CONSIDERATIONS FOR THE REALIZATION OF LPC USING THE META SYSTEM

The DLR's multiple swashplate control system (META) [44] is a fully IBC-capable control system without actuators in the rotating frame for tests with Mach-scaled model rotors.

With the concept patented in 2008 [45] and the IBC control procedure in 2013 [46] it has since been successfully tested on the DLR's rotor test bed [47], with first wind tunnel tests in the DNW's large low speed facility (LLF) planned in 2015 within the framework of the FTK-project.

While the system was tested with controlled frequencies (in the rotating system) of up to 6/rev, the introduction of (arbitrary) LPC functions poses new challenges regarding the overall control strategy of the system as well as actuator control.

In the course of further investigations regarding LPC, the limitations of the actuation system and its

controller as well as the mechanical system will be taken into account to allow the formulation of LPC functions, which can be realized using the existing system.

6. CONCLUSIONS AND OUTLOOK

- Basic numerical investigations with two different model rotors at μ=0.32 were conducted for different forms of Localized Pitch Control as well as 2/rev HHC.
- With Bo-105 model blades, LPC was found to perform superior to conventional 2/rev Higher Harmonic Control regarding both power reduction as well as simultaneous reduction of required power and vibration levels. Optimum LPC achieved power reductions of up to -3.62% (single objective optimization) as well as -2.26% in power and -57.3% in vibration levels (multi-objective optimization).
- While well suited for simultaneous power and vibration reduction, not all vibratory loads could be reduced by the optimized LPC functions. This issue is presumably resolvable by introducing a weighting factor into the calculation of the vibration cost function.
- Applied to a modern rotor blade with advanced geometry (especially at the blade tip), the achieved power reductions through LPC and HHC were significantly reduced and simultaneous reduction of rotor power and vibrational loads could not be achieved. While undoubtedly useful in terms of vibration reduction, active rotor control seems to offer only little potential for power reductions in combination with modern rotors.
- Future work is aimed at a more thorough understanding of the underlying physical phenomena responsible for the observed effects of LPC on required rotor power and vibrations. Furthermore the potential use of LPC for the reduction of pitch link loads during the occurrence of blade stall on the retreating side of the rotor, for example during maneuvers, will be examined.
- For possible experimental LPC investigations, the LPC functions will be modified to fit the requirements for realization on the DLR's multiple swashplate control system.

7. REFERENCES

[1]   A. Cler, "High-Speed Dauphin Fuselage Aerodynamics," in *Proceedings of the 15th European Rotorcraft Forum*, 1989, pp. 09–001 – 09–018.

[2]   W. Johnson, *Helicopter Theory*. Princeton University Press, 1980, p. 1089.

[3]   W. Stewart, "Second Harmonic Control on the Helicopter Rotor," *J. R. Aeronaut. Soc.*, vol. 2997, no. 2472, pp. 1–15, 1952.

[4]   P. J. Arcidiacono, "Theoretical Performance of Helicopters Having Second and Higher Harmonic Feathering Control," *J. Am. Helicopter Soc.*, vol. 6, no. 2, pp. 8–19, 1961.

[5]   K. Q. Nguyen, "Active suppression of stall on helicopter rotors by Army / NASA Rotorcraft Division," in *Proceedings of the 25th European Rotorcraft Forum*, 1999, pp. C13–1–C13–8.

[6]   R. P. Cheng, C. R. Theodore, and R. Celi, "Effects of Higher Harmonic Control on Rotor Performance," in *Proceedings of the 56th Annual Forum of the American Helicopter Society*, 2000, pp. 18–27.

[7]   R. P. Cheng and R. Celi, "Optimum Two-Per-Revolution Inputs for Improved Rotor Performance," *J. Aircr.*, vol. 42, no. 6, pp. 1409–1417, Nov. 2005.

[8]   K. Q. Nguyen and I. Chopra, "Effects of Higher Hamonic Control on Rotor Performance and Control Loads," *J. Aircr.*, vol. 29, no. 3, pp. 336–342, 1992.

[9]   P. Richter and A. Blaas, "Full Scale Wind Tunnel Investigation of an Individual Blade Control (IBC) System for the BO 105 Hingeless Rotor," in *Proceedings of the 19th European Rotorcraft Forum*, 1993, pp. G5–1 – G512.

[10] S. A. Jacklin, K. Q. Nguyen, A. Blaas, and P. Richter, "Full-Scale Wind Tunnel Test of a Helicopter Individual Blade Control System," in *Proceedings of the 50th Annual Forum of the Amiercan Helicopter Society*, 1994.

[11] M. Müller, U. T. P. Arnold, and D. Morbitzer, "On the Importance and Efficiency of 2/rev IBC for Noise, Vibration and Pitch Link Load Reduction," in *Proceedings of the 25th European Rotorcraft Forum*, 1999, pp. G4–1 – G4–12.

[12] S. A. Jacklin, A. Blaas, S. M. Swanson, and D. Teves, "Second Test of Helicopter Individual Blade Control System in the NASA Ames 40- by 80-Foot Wind Tunnel," in *Proceedings of the American Helicopter Society 2nd International Aeromechanics Specialists' Conference*, 1995.

[13] S. A. Jacklin, A. Blaas, D. Teves, and R. Kube, "Reduction of Helicopter BVI Noise, Vibration and Power Consumption through Individual Blade Control," in *Proceedings of the 51st Annual Forum of the American Helicopter Society*, 1995, pp. 662–680.

[14] T. R. Norman, C. Theodore, P. Shinoda, D. Fürst, U. T. P. Arnold, S. Makinen, P. Lorber, and J. O'Neill, "Full-Scale Wind Tunnel Test of a UH-60 Individual Blade Control System for Performance Improvement and Vibration, Loads and Noise Control," in *Proceedings of the 65th Annual Forum of the American Helicopter Society*, 2009.

[15] M. Achache and M. Polychroniadis, "Development of an Experimental System for Active Control of Vibration Helicopters," in *Proceedings of the 12th European Rotorcraft Forum*, 1986, no. 64.

[16] M. Polychroniadis and M. Achache, "Higher Harmonic Control: Flight Tests of an Experimental System on SA 349 Research Gazelle," in *Proceedings of the 42nd Annual Forum of the American Helicopter Society*, 1986, pp. 811–820.

[17] M. Polychroniadis, "Generalized Higher Harmonic Control - Ten Years of Aerospatiale Experience," in *Proceedings of the 16th European Rotorcraft Forum*, 1990.

[18] C. Kessler, D. Fürst, and U. T. P. Arnold, "Open Loop Flight Test Results and Closed Loop Status of the IBC System on the CH-53G Helicopter," in *Proceedings of the 59th Annual Forum of the American Helicopter Society*, 2003.

[19] D. Fürst and C. Kessler, "Closed Loop IBC-System and Flight Test Results on the CH-53G Helicopter," in *Proceedings of the 60th Annual Forum of the American Helicopter Society*, 2004.

[20] U. T. P. Arnold and D. Fürst, "Closed Loop IBC Results from CH-53G Flight Tests," *Aersosp. Sci. Technol.*, vol. 9, pp. 421–435, 2005.

[21] J. Götz, "Leistungsaspekte der Einzelblattsteuerung bei Hubschraubern," PhD Thesis, Technische Universität Carolo-Wilhelmina zu Braunschweig, 2005.

[22] H. Yeo, "Assessment of Active Controls for Rotor Performance Enhancement," in *Proceedings of the 62nd Annual Forum of the American Helicopter Society*, 2007, pp. 152–163.

[23] B. Malovrh and F. Gandhi, "Localized Individual Blade Root Pitch Control for Helicopter Blade-Vortex Interaction Noise Reduction," *J. Am. Helicopter Soc.*, vol. 55, no. 032007, pp. 32007–1 – 032007–12, 2010.

[24] F. Kody, E. Corle, M. D. Maughmer, and S. Schmitz, "Non-Harmonic Deployment of Trailing-Edge Flaps for Rotor-Performance Enhancement and Vibration Reduction," in *Proceedings of the 5th Decennial AHS Aerosmechanics Specialist' Conference*, 2014.

[25] B. G. van der Wall, "Analytic Formulation of Unsteady Profile Aerodynamics and its Application to Simulation of Rotors," ESA-TT-1244 (Translation of the Research Report DLR-FB 90-28, 1990), 1992.

[26] W. von Grünhagen, "Bestimmung der gekoppelten Schlagbiege-, Schwenkbiege- und Torsionsschwingungen für beliebige Rotorblätter mit Hilfe der Finite-Element-Methode (Computation of the coupled flap bending, lag bending and torsion oscillations for arbitrary rotor blades with," DFVLR IB 154-80/21, 1980.

[27] J. C. Houbold and G. W. Brooks, "Differential Equations of Motion for Combined Flapwise Bending, Chordwise Bending, and Torsion of Twisted Nonuniform Rotor Blades," NACA TN 3905, 1957.

[28] H. Wagner, "Über die Entstehung des dynamischen Auftriebes von Tragflügeln. (About the Development of Dynamic Lift of Wings)," *Zeitschrift für Angew. Math. und Mech.*, vol. 5, no. 1, pp. 17–35, 1925.

[29] H. G. Küssner, "Zusammenfassender Bericht über den instationären Auftrieb von Flügeln. (Summary Report about the Unsteady Lift of Wings)," *Luftfahrt-Forschung*, vol. 13, no. 12, pp. 410–424, 1936.

[30] R. L. Bisplinghoff, H. Ashley, and R. L. Halfman, *Aeroelasticity*. Reading, MA, USA: Addison-Wesley Publications Company Inc., 1957.

[31] D. Petot, G. Arnaud, R. Harrison, J. Stevens, D. Teves, B. G. van der Wall, C. Young, and E. Széchényi, "Stall Effects and Blade Torsion - An Evaluation of Predictive Tools," in *Proceedings of the 23rd European Rotorcraft Forum*, 1997.

[32] B. G. van der Wall and W. Geißler, "Experimental and Numerical Investigations on Steady and Unsteady Behaviour of a Rotor Airfoil with a Piezoelectric Trailing Edge Flap," in *Proceedings of the 55th Annual Forum of the American Helicopter Society*, 1999.

[33] B. G. van der Wall and J. Yin, "DLR's S4 Rotor Code Validation With HART II Data: The Baseline Case," in *Proceedings of the 1st International Forum on Rotorcraft Multidisciplinary Technology*, 2007.

[34] B. G. van der Wall and C. Göpel, "Über den Einfluss der Rotorversuchsstände ROTEST und ROTOS auf die Rotordurchströmung im DNW. (About the Influence of the Rotor Test Rigs ROTEST and ROTOS on the Flow in the Rotor Disk in DNW)," DLR-Mitteilung 91-16, 1991.

[35] B. G. van der Wall, A. Bauknecht, S. N. Jung, and Y. H. You, "Semi-Empirical Physics-Based Modeling of Fuselage-Rotor and Fuselage-Wake Interferences for Comprehensive Codes," in *Proceedings of the 70th Annual Forum of the American Helicopter Society*, 2014.

[36] T. S. Beddoes, "A Wake Model for High Resolution Airloads," in *Proceedings of the 1st AHS/ARO International Conference on Rotorcraft Basic Research*, 1985.

[37] K. W. Mangler and H. B. Squire, "The Induced Velocity Field of a Rotor," *ARC R&M*, no. 2642, 1950.

[38] B. G. van der Wall, "Helicopter Rotor BVI Airloads Computation Using Advanced Prescribed Wake Modeling," in *Proceedings of the 29th AIAA Applied Arerodynamics Conference*, 2011.

[39] B. G. van der Wall, B. Junker, C. L. Burley, T. F. Brooks, Y. H. Yu, C. Tung, M. Raffel, H. Richard, W. Wagner, E. Mercker, K. Pengel, H. Holthusen, P. Beaumier, and Y. Delrieux, "The HART II Test in the LLF of the DNW - a major step towards rotor wake understanding," in *Proceedings of the 28th European Rotorcraft Forum*, 2002.

[40] B. Enenkl, V. Klöppel, D. Preißler, and P. Jänker, "Full Scale Rotor With Piezoelectric Actuated Blade Flaps," in *Proceedings of the 28th European Rotorcraft Forum*, 2002.

[41] B. Benoit, A.-M. Dequin, K. Kampa, W. von Grünhagen, P.-M. Basset, and B. Gimonet, "HOST: A General Helicopter Simulation Tool for Germany and France," in *Proceedings of the 56th Annual Forum of the American Helicopter Society*, 2000.

[42] R. Storn and K. Price, "Differential Evolution - A simple and efficient adaptive scheme for global optimization over continuous spaces," TR-95-012, 1995.

[43] B. J. A. Nelder and M. R, "A simplex method for function minimization," *Comput. J.*, vol. 7, no. 4, pp. 308–313, 1964.

[44] R. Bartels, P. Küfmann, and C. Kessler, "Novel Concept for Realizing Individual Blade Control (IBC) for Helicopters," in *Proceedings of the 36th European Rotorcraft Forum*, 2010.

[45] B. G. van der Wall and R. Bartels, "Patent für eine Hubschrauber-Rotorsteuereinrichtung," 10 2006 030 0892008.

[46] P. Küfmann, "Patent für ein Verfahren zum Ermitteln von Stellgrößen," 10 2010 024 089 842013.

[47] P. Küfmann, R. Bartels, and O. Schneider, "DLR's Multiple Swashplate Control System: Operation and Preliminary Testing," in *Proceedings of the 38th European Rotorcraft Forum*, 2012.